Journal of Alloys and Compounds, 204 (1994) 109–118
JALCOM 908

New oxides of the filled-Ti_2Ni type structure

Richard Mackay, Gordon J. Miller and Hugo F. Franzen
Ames Laboratory–DOE and Department of Chemistry, Iowa State University, Ames, IA 50011 (USA)

(Received July 20, 1993)

Abstract

The metal atom ordering and oxygen occupancy of four compounds of the filled-Ti_2Ni type structure have been determined by single-crystal X-ray diffraction studies. Three additional phases have been identified and indexed from powder X-ray diffraction data. All the phases crystallize in space group $Fd\bar{3}m$ with the following compositions: Zr_4Ni_2O ($a = 12.1970(9)$ Å), $Zr_6Ni_4Ti_2O_{0.6}$ ($a = 12.0299(9)$ Å), Nb_6Ni_6O ($a = 11.2117(5)$ Å), and $Nb_6Ni_4Ta_2O_2$ ($a = 11.5813(3)$ Å). Phases identified using powder data are Nb_4Ni_2O ($a = 11.5933(3)$ Å), Zr_4Cu_2O ($a = 12.2659(7)$ Å), and $Zr_6Co_4Ti_2O$ ($a = 11.8649(9)$ Å). A comparison of the structures and oxygen occupancies is presented, as well as tentative explanations based on results of extended Hückel calculations. The role of interstitial oxygen as an electron acceptor and its effect on metal–metal bonding are considered.

1. Introduction

The Ti_2Ni, the filled-Ti_2Ni, and the related η carbide type structures have been known for some time [1]. Much of the earlier work revealed the variety of combinations of metals for which this structure forms. The simplicity of the formula conceals the subtleties and complexities in the chemistry of these phases. It is a frequently found structure of binary intermetallics of stoichiometry A_2B [2]. Many of these binary intermetallics can incorporate light interstitial atoms. Many more phases form only in the presence of these interstitial atoms, commonly C [3–6], N [7–9], O [10–12], and even H [13]. A review of the literature and list of reported phases suggests that there is no general explanation for the variability in compositions and there is no known correlation of interstitial atom site occupancy and metal:metal ratio. Although much of the work was done a number of years ago, significant recent reports in the literature prompt further investigation of these phases [6, 9, 12–14]. Many reports are based on X-ray powder diffraction data, with the inherent difficulty in refining parameters for light interstitial elements. Some neutron diffraction work has been reported [6, 14, 15]. No single-crystal work has been previously reported for any of these interstitial stabilized phases. Presumably this is because of the difficulty in forming single crystals suitable for diffraction experiments. The crystals examined here were all very small, and the successful refinements were possible because of the high X-ray beam intensity from a diffractometer with a rotating anode X-ray generator.

The filled-Ti_2Ni type structure crystallizes in space group $Fd\bar{3}m$, and the unit cell contains 96 metal atoms. Adopting the notation of Newsam *et al.* [6], the general formula for the oxides is written $M^f_6M^c_4M^d_2O^c_2O^a_1$. The superscript letters are those of the Wyckoff symbol for the crystallographic site occupied by the superscripted atoms. The subscripts are based on the unit cell formula with $Z = 8$. For a ternary compound M^f and M^e are different transition metals, and M^d may be the same as either M^f or M^e, depending on the system being considered. The transition metal M^f is always to the left of the M^e metal atom in the periodic table. When the f and d sites are occupied by the same metal the metal:metal ratio is 8:4, or 2:1. When the e and d sites are occupied by the same metal the metal:metal ratio is 6:6, or 1:1. No mixing on the M^d site has been observed. Oxygen is reported to occupy either the 16c site, in which it fills distorted octahedra, or the 8a site, filling regular octahedra.

The structure of the large cubic unit cell has been described in the literature in two general schemes. In the first scheme, the cell is built up of alternating subunits, as depicted in Fig. 1. The octahedra of M^f and tetrahedra of M^e atoms are outlined. The oxygen atoms can be seen in Fig. 1(a) between the outlined octahedra. This is a distorted octahedral site, sharing opposite faces with the regular octahedra. The M^d metal atoms can be seen in Fig. 1(b) capping the faces of the M^e tetrahedra. The second scheme describes the structure in terms of two interpenetrating networks, as depicted in Fig. 2. Figure 2(a) illustrates a network of face-sharing octahedra which alternately share two and

SSDI 0925-8388(93)00908-H

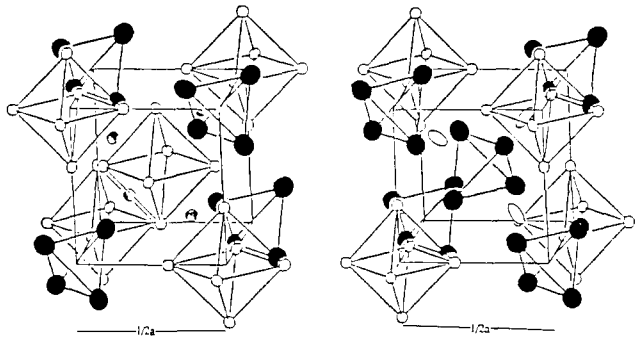

Fig. 1. View of individual subunits making up the unit cell of Zr_4Ni_2O: (a) Subunit centered by zirconium octahedron; (b) subunit centered by nickel tetrahedron.

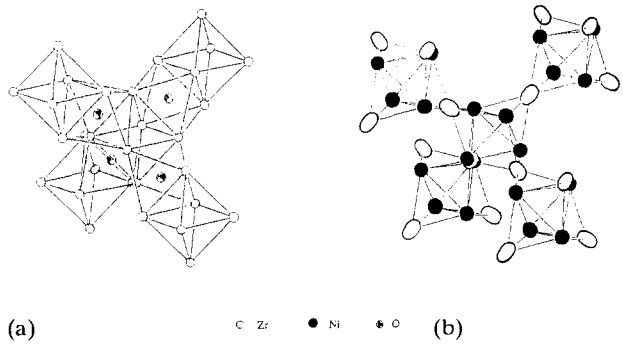

Fig. 2. (a) Network of face-sharing zirconium octahedra in Zr_4Ni_2O. Shaded octahedra are centered by oxygen, unshaded octahedra are empty. (b) Network of stellae quadrangulae in Zr_4Ni_2O. Nickel tetrahedra are shaded.

four faces. The octahedra shown are alternately centered by oxygen and empty. The face-sharing octahedra form rings made up of 12 octahedra. The void spaces within and between these rings are filled by an interpenetrating network of corner-sharing stellae quadrangulae (Fig. 2(b)) [16, 17].

2. Experimental details

All chemicals were used as they were received from the supplier, except as noted below: Zr (0.25 mm foil, Alfa Products, 99.9%); Zr (−20 to +60 mesh, Johnson Matthey, 99.9%); Ti (Ames Laboratory); ZrO_2 (Johnson Matthey Puratronic, 99.9975%); NiO (Johnson Matthey Puratronic, 99.998%); Nb (−325 mesh, Alfa Products, 99.8%); Ta (60 mesh, Johnson Matthey, 99.98%); Ni (foil, Inco, 99.99%); Ni (powder, Fisher Scientific, purified); Cu (ribbons, J.T. Baker Chemical Co., 99.98%); Co (pieces, Alfa, 99.5%); $NaClO_4$ (GFS Chemical Co., 99%). Ni received from Inco was arc melted under argon, and rolled into a foil. Analysis was carried out after this treatment. The foils were cleaned in acid solutions to remove surface oxides prior to their use.

Samples were prepared by two general techniques. The first technique consisted of arc melting the metals and the oxide of either zirconium or nickel. The samples were then annealed under vacuum in an induction furnace. This technique often resulted in a mixture of phases. ZrO_2 was always present as a minor phase in the zirconium compounds. Other minor phases present in various samples were Zr_3NiO and the oxygen-stabilized cubic Laves phase, $ZrNi_2O_x$ [18]. Apparently, the Laves phase has a low melting point (less than 1000 °C) and the presence of this phase masks the refractory nature of this family of compounds. Samples free of this phase remained solid when annealed at 1250–1275 °C. Samples containing niobium all had NbO as a minor phase, and some also had Nb_7Ni_6 present. The desired phase was present on annealing at temperatures as low as 1000 °C, but most samples were annealed at 1250 °C. The melting point of Nb_7Ni_6 is 1290 °C.

A second method was used successfully for the preparation of a nearly single-phase sample of Zr_4Ni_2O. Only the two strongest lines of ZrO_2 were barely visible in the powder X-ray diffraction pattern of this phase. A sample of Zr and Ni was arc melted, as before, and then ground to small pieces. The metal and an appropriate amount of oxidizing agent, $NaClO_4$, were sealed in an evacuated fused silica tube. On heating to 600 °C for 4 days in a tube furnace the perchlorate decomposed, and crystals of NaCl formed at the cool end of the tube. The resulting oxide was crushed to a fine powder and pressed into a pellet before annealing as before.

X-ray powder diffraction techniques were used to identify the phases present, and to determine accurate lattice parameters. Powder diffraction films were obtained using a vacuum Guinier camera FR552 (Enraf-Nonius, Delft, the Netherlands) with Cu $K\alpha_1$ radiation. Lattice parameters were determined by a least-squares refinement of indexed line positions calibrated by an internal silicon standard (NIST).

Single-crystal X-ray diffraction data collection was carried out on a Rigaku AFC6R diffractometer, with Mo $K\alpha$ radiation ($\lambda = 0.710\,69$ Å). The structures were solved by direct methods and refined using the SHELXS [19] and TEXSAN [20] software packages. All crystals were refined in space group $Fd\bar{3}m$. Details of crystal data are listed in Table 1.

A Quantum Design superconducting quantum interference device magnetometer was used to check for superconductivity and to measure magnetic behavior at a field of 3 T over the temperature range 6–298 K.

Elemental analysis of the zirconium nickel oxides by energy-dispersive spectroscopy (EDS) was performed on a JEOL JSM-840 electron microscope.

TABLE 1. Single-crystal data of new filled-Ti_2Ni type phases

Formula	Zr_4Ni_2O	$Zr_6Ni_4Ti_2O_{0.6}$	Nb_6Ni_6O	$Nb_6Ni_4Ta_2O_2$
a (Å)	12.1970(9)	12.0299(9)	11.2117(5)	11.5813(3)
V (Å^3)	1814.5(4)	1740.9(4)	1409.3(2)	1553.4(1)
Z	16	8	8	8
d_{calc} (g cm^{-3})	7.295	6.747	8.742	10.390
Crystal size (μm^3)	40×50×70	50×50×100	40×40×40	30×40×50
μ(Mo Kα) (cm^{-1})	167	169	246	494
Data collection range 2θ (deg)	0–60	0–55	0–55	0–60
Number of reflections measured	768	579	482	1253
Number of unique data, total with $F_o^2 > 3\sigma(F_o^2)$	112	87	79	101
Number of parameters refined	13	15	11	15
Transmission factor ratio (maximum:minimum)	1.116	1.168	1.146	1.179
R^a	0.020	0.029	0.017	0.022
R_w^b	0.024	0.031	0.023	0.029
GOF^c	1.019	0.995	0.980	1.026
Largest peak (e Å^{-3})	1.59	1.20	0.88	1.54
Largest negative peak (e Å^{-3})	−1.17	−1.31	−1.04	−3.19

$^a R = \Sigma||F_o| - |F_c||/\Sigma|F_o|$.
$^b R_w = [\Sigma w(|F_o| - |F_c|)^2/\Sigma w|F_o|^2]^{1/2}$; $w = 1/\sigma^2(|F_o|)$.
$^c \text{GOF} = (\Sigma(|F_o| - |F_c|)/\sigma_i)/(N_{\text{obs refl}} - N_{\text{parameters}})$.

3. Results

Interest in the Ti_2Ni-type structures arose from a study of the interstitially stabilized intermetallic phases that form in the Zr–Ni system [21–23]. Two experimental results deserved attention. First, previous work on the Zr–Ni–O phase diagram in an intentional search for this cubic phase indicated that it does not exist in equilibrium at 950 °C [24]. It does exist, however, at 1275 °C, the annealing temperature used in these experiments. This is thus an example of a high temperature solid phase which decomposes at lower temperature, in this case probably to Zr_3NiO and Ni. Second, there was a noticeable shift in lattice parameters for this phase in several of the samples, as observed in the films of the powder diffraction patterns taken on a Guinier camera. A single crystal was chosen from both a sample with the larger lattice parameter and a sample with the smaller lattice parameter. The results for the data refinement of the larger cell correspond to the data reported for Zr_4Ni_2O in Table 2. The preliminary solution for the smaller cell was also based on a Zr–Ni–O ternary system, and required Ni vacancies on the 16d site for a suitable refinement, giving a stoichiometry of $Zr_6Ni_{6-x}O$. This solution was corrected when elemental analysis by EDS revealed the presence of titanium, which could be detected in samples prepared with a zirconium starting material which unexpectedly contained significant amounts of titanium Placing Ti in the 16d site in the structure solution improved the refinement significantly, and the final refinement showed full occupancy on all the metal sites. The results for $Zr_6Ni_4Ti_2O_{0.6}$ are also in Table 2. Efforts to synthesize a compound of stoichiometry Zr_6Ni_6O, without titanium, were unsuccessful.

A systematic check for a solid solution between Zr_4Ni_2O and Ti_4Ni_2O was not performed, but, for low concentrations of titanium, the titanium preferentially substitutes on the 16d site. Furthermore, the oxygen partially occupies both interstitial sites in the sample containing titanium, with total oxygen occupancy given by the formula $Zr_6Ni_4Ti_2O_{0.6}$. The refinement was carried out considering the following possible solutions: Zr_6Ni_4Ti (no oxygen), $Zr_6Ni_4Ti_2O_{1-x}$ (variable oxygen occupancy on the 8a site only), $Zr_6Ni_4Ti_2O_{2-x}$ (variable oxygen occupancy on the 16c site only), and $Zr_6Ni_4Ti_2O_{3-x}$ (variable oxygen occupancy on both the 8a and the 16c sites). By careful comparison of each of the refinement solutions, according to Hamilton's test [26], the solution with both sites partially occupied is correct with a 95% level of confidence.

Conflicting reports exist for the Zr_4Co_2O phase. Nevitt and Downey [24] did not find this phase in determining the 950 °C isothermal section of this ternary system. Holleck and Thümmler [8] include Zr_4Co_2O ($a = 12.18$ Å) in a list of phases observed. This phase did not form in samples annealed at 1100 °C. However, it was observed to form at this temperature in samples prepared with the titanium-contaminated zirconium. By analogy with the substitution of Ti in Zr_4Ni_2O, this is formulated as $Zr_6Co_4Ti_2O$ ($a = 11.8649(9)$ Å), with undetermined oxygen occupancy.

TABLE 2. Final atomic parameters from single-crystal refinement

Atom	Site	x	y	z	B_{eq} (Å^2)[a]
Zr_4Ni_2O					
Zr1	48f	0.18517(8)	0.0	0.0	0.51(1)
Ni	32e	0.8396(1)	0.8396	0.8396	1.2716(5)
Zr2	16d	0.625	0.625	0.625	1.5990(5)
O[b]	16c	0.125	0.125	0.125	0.562(2)
$Zr_6Ni_4Ti_2O_{0.6}$					
Zr	48f	0.1901(1)	0.0	0.0	0.73(4)
Ni	32e	0.8326(2)	0.8326	0.8326	1.1795(7)
Ti	16d	0.625	0.625	0.625	1.430(1)
O[c]	16c	0.125	0.125	0.125	1.17(3)
O[c]	8a	0.0	0.0	0.0	0.98(3)
Nb_6Ni_6O					
Nb	48f	0.1996(1)	0.0	0.0	0.47(2)
Ni1	32e	0.8317(1)	0.8317	0.8317	0.3289(4)
Ni2	16d	0.625	0.625	0.625	0.4602(6)
O[b]	8a	0.0	0.0	0.0	0.497(4)
$Nb_6Ni_4Ta_2O_2$					
Nb[d]	48f	0.1867(1)	0.0	0.0	0.48(4)
Ni	32e	0.8311(1)	0.8311	0.8311	0.422(1)
Ta[e]	16d	0.625	0.625	0.625	0.3491(6)
O[b]	16c	0.125	0.125	0.125	1.154(5)
Idealized metal positions[f]					
M1	48f	0.1875	0.0	0.0	
M2	32e	0.8250	0.8250	0.8250	

[a] $B_{eq} = \frac{8\pi^2}{3} \Sigma_1^3 \Sigma_1^3 U_{ij} a_i^* a_j^* \vec{a}_i \vec{a}_j$.

[b] Refined with full oxygen occupancy.

[c] Refinement of the oxygen occupancy gave results of the 16c site being 18(6)% occupied and the 8a site 24(6)% occupied.

[d] Refined with mixed Nb–Ta occupancy: Nb, 82(2)%; Ta, 18(2)%.

[e] Refined with mixed Ta–Nb occupancy: Ta, 61(3)%; Nb, 39(3)%.

[f] From ref. 25.

The results of electronic structure calculations on Zr_4Ni_2O indicated the presence of empty bonding orbitals. This suggested the possibility of adding electrons to the system by substituting copper for nickel or niobium for zirconium. The synthesis of both Zr_4Cu_2O and Zr_6Cu_6O was attempted at temperatures between 900 and 1100 °C. With the Zr:Cu starting ratio of 2:1, the powder pattern indicated the presence of the desired phase as well as binary Zr_2Cu as a minor phase. When the starting Zr:Cu ratio was 1:1 the products were the cubic phase and the binary Zr_3Cu_8. The lattice parameters of the Ti_2Ni-type phase differed only slightly in all the samples made. For the nearly single-phase sample made with a 2:1 starting metal ratio, $a = 12.2659(7)$ Å. The smallest cell edge measured for the cubic phase with the 1:1 starting ratio was $a = 12.2615(6)$ Å. This leads to the conclusion there is only the one phase, Zr_4Cu_2O, with perhaps a slightly varying oxygen content accounting for the differences in observed cell lengths. Characterization of these phases was performed by X-ray powder diffraction photographs. The oxygen is assumed to occupy the 16c site. A significant shortening in the unit cell is observed when Ti is added to form $Zr_6Cu_4Ti_2O$ ($a = 12.16(2)$ Å).

The existence of the two distinct phases in the Nb–Ni–O system reported previously is confirmed [8]. This contrasts with the Nb–Ni–C system for which only the Nb_4Ni_2C phase is noted in the 1100 °C isotherm of the ternary phase diagram [27]. Single-crystal X-ray diffraction data for Nb_6Ni_6O ($a = 11.2117(5)$ Å) were used to determine oxygen occupancy in this phase which had been reported as Nb_3Ni_3O ($a = 11.20$ Å) Nb_4Ni_2O has lattice parameter $a = 11.5933(3)$ Å (previously reported with $a = 11.58$ Å). Comparison of oxygen occupancies in the Nb–Ni–O samples is incomplete because single crystals of Nb_4Ni_2O have not been found. The difference in lattice parameters clearly indicates the existence of two distinct phases. Samples of the oxides have been prepared which contain both phases in an equilibrium mixture. The existence of the two distinct phases emphasizes that the 16d site is occupied entirely either by niobium or by nickel, but not by both in a solid solution on this metal site.

Ta_4Ni_2O is reported by Holleck and Thümmler [8]. Kotyk and Stadelmaier [7] find that this phase only exists with nitrogen present, as either Ta_4Ni_2N or the mixed $Ta_4Ni_2(O,N)$, but not as the pure oxide. Efforts to synthesize both Ta_4Ni_2O and Ta_6Ni_6O, annealing at temperatures between 1430 and 1550 °C, resulted in mixtures of binary phases. However, noting the effect of titanium in the zirconium compounds, the synthesis of mixed Ta–Nb compounds was attempted. Both of the starting compositions $Ta_6Ni_4Nb_2O_2$ and $Nb_6Ni_4Ta_2O_2$ were tried. Only the latter formed the cubic phase, at 1550 °C, with $(Ta,Nb)_7Ni_6$ present as a minor phase. A single crystal was selected for study by X-ray diffraction. A ψ scan suitable for absorption correction in the refinement process was not collected. As an empirical absorption correction (DIFABS) did not improve the refinement, no correction was applied in the final refinement. The Nb and Ta occupancies were allowed to vary in the final steps of the refinement, resulting in a final stoichiometry of $(Nb_{0.82}Ta_{0.18})_6Ni_4(Ta_{0.61}Nb_{0.39})_2O_2$, or $Nb_{5.7}Ni_4Ta_{2.3}O_2$.

Crystal data for all the single-crystal refinements are listed in Table 1. Positional and thermal parameters for the four single-crystal refinements are listed in Table 2. Interatomic distances are shown in Table 3. Table 4 summarizes all of the phases identified in this study and corresponding lattice parameters. Anisotropic displacement parameters and structure factor tables are available in the supplementary material.

Zr_4Ni_2O, $Nb_6Ni_4Ta_2O_2$, Nb_4Ni_2O, and Nb_6Ni_6O were checked for superconductivity down to 6 K. No transition was observed. Magnetic measurements of the Zr_4Ni_2O and $Nb_6Ni_4Ta_2O_2$ phases from 6 to 298 K at a field

TABLE 3. Interatomic distances in new filled-Ti_2Ni type phases

	Zr_4Ni_2O	$Zr_6Ni_4Ti_2O$	Nb_6Ni_6O	$Nb_6Ti_4Ta_2O_2$
M1[a]–O1 ×1	–	2.287(2)	2.238(1)	–
O2 ×2	2.2776(7)	2.266(2)	–	2.162(1)
Ni ×2	2.7832(9)	2.861(2)	2.691(1)	2.774(1)
Ni ×2	3.152(1)	3.075(2)	2.773(1)	2.9912(6)
M2 ×2	3.164(1)	3.078(1)	2.7920(8)	2.999(1)
M1 ×4	3.194(1)	3.175(1)	2.915(1)	3.058(1)
M1 ×4	3.248(1)	3.234(1)	3.165(1)	3.075(1)
Ni–M2 ×3	2.688(1)	2.600(1)	2.4170(6)	2.4928(6)
Ni ×3	3.0910(9)	2.811(5)	2.591(1)	2.657(1)
M1 ×3	2.7832(9)	2.861(2)	2.691(1)	2.774(1)
M1 ×3	3.152(1)	3.075(2)	2.773(1)	2.999(1)
O1 ×1	–	3.488(3)	3.268(2)	–
O2 ×3	3.534(1)	3.590(2)	–	3.388(1)
M2[b]–Ni ×6	2.6878(8)	2.600(1)	2.4170(6)	2.4928(6)
M1 ×6	3.164(1)	3.078(1)	2.7920(8)	2.9912(6)
O1[c]–M1 ×6	–	2.287(2)	2.238(1)	–
Ni ×4	–	3.488(3)	3.268(2)	–
O2[d]–M1 ×6	2.2776(7)	2.266(2)	–	2.162(1)
Ni ×6	3.534(1)	3.590(2)	–	3.388(1)

[a]M1 = Zr or Nb in 48f.
[b]M2 = Zr, Ti, Ni, or Ta in 16d.
[c]O1 = O in 8a.
[d]O2 = O in 16 c.

TABLE 4. Lattice parameters for all new filled-Ti_2Ni type phases found

Composition	a (Å)
Zr_4Cu_2O	12.2659(7)
Zr_4Ni_2O	12.1970(9)
$Zr_6Ni_4Ti_2O_{0.6}$	12.0299(9)
$Zr_6Co_4Ti_2O$	11.8649(9)
Nb_4Ni_2O	11.5933(3)
$Nb_6Ni_4Ta_2O_2$	11.5813(3)
Nb_6Ni_6O	11.2117(5)

of 3 T show that they are both paramagnetic. The latter sample contained approximately 10% of an impurity phase of the Nb_7Ni_6 type. No magnetic measurements of Nb_7Ni_6 or Ta_7Ni_6 have been reported, and it is possible this phase is paramagnetic also.

4. Electronic structure calculations

Electronic structure calculations were carried out on the Zr_4Ni_2O phase. Calculations were also performed on Nb_6Ni_6O in an attempt to correlate the oxygen ordering with the metal ratios. The calculations were of the extended Hückel type using the tight binding approximation. The atomic parameters used for the calculations are listed in Table 5. The valence state ionization potentials H_{ii} for the metals were obtained

TABLE 5. Atomic parameters used for extended Hückel calculations

Atom	Orbital	H_{ii} (eV)	ζ_1[a]	ζ_2[a]	c_1[b]	c_2[b]
Zr	4d	−6.72	3.84	1.505	0.6213	0.5798
	5s	−7.06	1.82			
	5p	−3.68	1.78			
Ni	3d	−8.43	5.75	2.20	0.5817	0.5800
	4s	−6.76	1.925			
	4p	−3.03	1.925			
O	2s	−32.3	2.275			
	2p	−14.8	2.275			

[a]Exponent in the double ζ function for d orbitals.
[b]Coefficients to exponential terms.

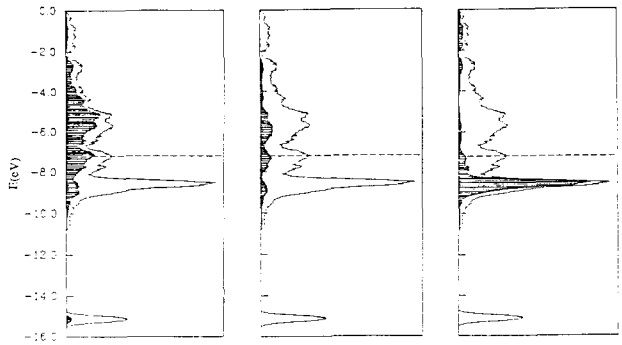

Fig. 3. Projection of individual atomic contributions on total DOS for Zr_4Ni_2O: (a) projection of Zr1 on total DOS; (b) projection of Zr2 on total DOS; (c) projection of Ni on total DOS.

from a charge iteration calculation on the binary Zr_2Ni, Al_2Cu-type structure. Other parameters were taken from previous work [28–32].

General features of the density of states (DOS) plots of Zr_4Ni_2O can be seen in Fig. 3, which shows the projection of the contribution of the metal atoms to the total DOS. Figure 3(a) shows the projection of the Zr1 atoms on the total DOS. These are the zirconium atoms which make up the network of face-sharing octahedra. The oxygen atoms center an alternating set of these octahedra, and the mixing of zirconium with the oxygen p band is seen at low energy. The broad band at higher energy has principally zirconium d character. Figure 3(b) similarly shows the broad d band of the zirconium atoms occupying the M^d site. Figure 3(c) shows the narrow nickel d band, with nickel character extending up through the conduction band to higher energy. The Fermi level indicated by the broken line is in the middle of the conduction band. In all the calculations, the Zr1 atoms were placed on the "idealized" atom position [25], making all octahedral sites equal in size to avoid biasing the results and favoring a site for oxygen occupancy dependent on size

factors. The nickel position was shifted to be between the observed atom position and the "idealized" atom position.

Table 6 compares the effect on the Fermi energies and total energies of adding oxygen to the hypothetical cubic binary; first to the sixteenfold site, as observed in the single-crystal refinement, and then to the other possible octahedral site, an eightfold site. The bottom row of Table 6 is the total energy gain per oxygen atom added to the system. That is to say, the formation of Zr_4Ni_2O by adding oxygen to Zr_4Ni_2 decreases the total energy of the system from −1225.62 eV to −1775.43 eV, or by −549.81 eV. There are four oxygen atoms in the primitive unit cell, so the energy change per oxygen atom is one-fourth the total change, or −137.45 eV. By comparing the change per oxygen atom, the results of adding different amounts of oxygen can be compared. The table shows the two results differ by only 0.31 eV per oxygen atom. The calculated preferred ordering is in favor of the observed result, but it is doubtful whether the difference is significant within the errors of the calculations associated with the approximations of the extended Hückel method.

The results of the single-crystal refinement of Nb_6Ni_6O show that the oxygen can occupy the eightfold site in the structure. Not only is the oxygen occupancy in this compound different from that in Zr_4Ni_2O, but the metal:metal ratio is also different. Calculations were performed on the compound Nb_6Ni_6O, using for niobium the zirconium parameters from the charge iteration. Table 7 lists the energies associated with each of these phases with different amounts of oxygen. The changes in energy per oxygen atom are such that the observed phase is again favored, but by only 0.15 eV. In addition to the uncertainty within the calculations, the calculations do not allow for non-stoichiometry, or partial filling of the sites. If only half of the sixteenfold sites are occupied by oxygen, the stoichiometry is the same as for the observed phase, Nb_6Ni_6O. For the calculation

TABLE 6. Fermi energy and total energy of calculated phases

	Zr_4Ni_2	$Zr_4Ni_2O_{1/2}$	Zr_4Ni_2O
Fermi energy E_F (eV)	−7.242	−7.212	−7.205
Total energy E_T (eV)	−1225.62	−1499.91	−1775.43
ΔE_T (oxygen atom)		−137.14	−137.45

TABLE 7. Fermi energy and total energy of calculated phases

	Nb_6Ni_6	Nb_6Ni_6O	$Nb_6Ni_6O_2$
Fermi energy E_F (eV)	−7.087	−7.027	−6.817
Total energy E_T (eV)	−1515.37	−1789.10	−2062.22
ΔE_T (oxygen atom)		−136.86	−136.71

TABLE 8. Overlap populations for Zr_4Ni_2O

Atomic interaction	Overlap population	Interatomic distance (Å)
Zr2–Zr1	0.1646	3.12
Zr1–Ni	0.1347	2.76
Zr1–O	0.1089	2.27
Zr2–Ni	0.1014	2.67
Zr1–Zr1	0.0980	3.21
Zr1–Ni	0.0412	3.10

of this phase, then, two of the four oxygen sites were filled, and the other two were empty. The total energy for this phase was −1789.01 eV, resulting in a stabilization of −136.82 eV per oxygen atom. This is different by only 0.04 eV from the calculated energy for the observed structure. These results suggest that the important consideration may not be which site is occupied, but the amount of oxygen the system requires for maximum stabilization.

It should be noted that when O atoms are added to both binary intermetallics, the calculated Fermi energies rise. In general, the valence orbitals of main group interstitial atoms interact with bonding orbitals within early transition metal and rare earth clusters [33]. These levels occur at the bottom of the conduction band in intermetallic solids. The O interstitials, through their orbital interactions, push some of these cluster bonding levels to high energy, and we observe slight increases in the position of the Fermi level. In terms of chemical bonding ideas, these intermetallics gain electronic energy by forming metal–interstitial bonds at the expense of metal–metal bonds in the cluster.

Crystal orbital overlap population (COOP) curves were calculated for the interactions in Zr_4Ni_2O. The calculated overlap populations are tabulated in Table 8, appropriately weighted to reflect the number of each symmetry unique bond. Nickel–nickel overlap population was very low, *ca.* 0.001, and is not included in the table. Each of the COOP curves for metal–metal interactions shows empty bonding orbitals above the Fermi level. The only indication of antibonding character at the Fermi level was in the COOP curve for Zr1–O interactions. As mentioned previously the calculation of empty bonding levels was the motivation for the synthesis of more electron-rich compounds than Zr_4Ni_2O.

5. Discussion

The Ti_2Ni-type structure has been described in terms of two interpenetrating three-dimensional networks made of idealized octahedra and tetrahedra [25]. With

the idealized parameters listed in Table 2, M1 is at $(x, 0, 0)$ with $x = 0.1875$, and all the face-sharing octahedra are exactly the same size. When x deviates from this value the octahedral centred at an 8a site maintain ideal octahedral symmetry, but the other octahedra, centered at a 16c site, lose their fourfold symmetry, and become distorted octahedra, or, more precisely, trigonal antiprisms. The direction of the deviation of x from ideality appears to be related to the oxygen occupancy. The octahedra, regular or distorted, centered by oxygen are expanded. When oxygen occupies the 8a site, at the origin, the expansion of the regular octahedra corresponds to an increased value for x (compare Nb_6Ni_6O, with $x = 0.1996$, and ideal $x = 0.1875$). Occupancy of the 16c site causes expansion of the distorted octahedra, or trigonal antiprisms, and a corresponding decrease in x (compare $x = 0.1852$ in Zr_4Ni_2O and $x = 0.1867$ in $Nb_6Ti_4Ta_2O_2$, with ideal $x = 0.1875$). The expansion of the oxygen-centered octahedra can be interpreted as resulting from the filled antibonding metal–oxygen orbitals, as calculated in the COOP curves. There appears to be a correlation of metal atom position with interstitial site occupancy. This is a useful crystal–chemical correlation, given the inherent difficulty of refining light atom positions by X-ray diffraction techniques. For example, this suggests a reinvestigation of a recent report of Mo_3Fe_3N [9]. The positional parameters for the molybdenum suggest that the nitrogen occupies the 8a site, with the corresponding formula Mo_6Fe_6N.

Interpenetrating the octahedral network is another network made of corner-sharing stellae quadrangulae. In the compounds studied here the central tetrahedron is always made of Ni, on the 32e site, and the other atoms are the metals on the 16d site, which cap the faces of the Ni_4 tetrahedra. None of these tetrahedra is centered by interstitial atoms. Hyde and Andersson list the idealized position for the metal atom as $x = 0.4250$ [25]. This has been converted to the alternate but equivalent value of 0.8250 for comparison with the refinement results. The refined Ni atom positions on the 32e site vary from $x = 0.8311$ to $x = 0.8396$. The effect of increasing the x parameter is to enlarge the central nickel tetrahedron. A look at the distances in Table 3 shows these units are far from regular stellae quadrangulae. In all cases the central Ni_4 tetrahedron is expanded ($d_{Ni-Ni} > d_{Ni-M2}$). Zr_4Ni_2O exhibits the largest departure from ideality. For the ideal structural arrangement of this compound, $d_{Ni-Ni} = 2.5873$ Å. The observed distance is much larger, $d_{Ni-Ni} = 3.0910$ Å. In elemental nickel $d_{Ni-Ni} = 2.4916$ Å. The distance between the tetrahedral nickel atoms and the zirconium atoms in the octahedral network consequently decreases considerably from the ideal. Compare the observed $d_{Zr1-Ni} = 2.783$ Å in Zr_4Ni_2O with the ideal $d_{Zr1-Ni} = 3.0224$ Å. This expansion of the Ni_4 tetrahedron suggests that Ni–Ni interactions are weaker, relative to Zr–Ni interactions, than would be the case in the idealized structure. This suggests that the visual description of the structure in terms of two interpenetrating networks does not accurately portray the chemical interaction between the two networks. The icosahedral units around the M2 atoms at the 16d sites are exactly the bonding connections between the two networks [9, 34]. The interactions between the two interpenetrating networks are as important as the interactions within a network.

Periodic equipotential surfaces and periodic zero potential surfaces have been calculated for this space group [35]. The potential surfaces of appropriate coulombic fields are very similar in shape to minimal surfaces, but can be correlated to the spatial distribution of the electrons, and hence correlated to physical properties. For the Ti_2Ni structure the potential surface resides between the two interpenetrating networks. One can assume that the most weakly bound electrons are located closest to the potential surface. In a metal, these are the conduction electrons. This view of potential surfaces in no way contradicts the finding here of significant interaction between the two structural networks.

It is interesting to note some structural similarities with other phases here. A two-dimensional analogue to the three-dimensional network of face-sharing zirconium octahedra is seen in both the κ phase [22] and the new $Zr_6Ni_6TiSiO_{1.8}$ structure [23]. In each case, rings of twelve face-sharing zirconium octahedra form. In the case of all three of these structures, icosahedral units fill the void spaces and link the octahedral networks.

The results of this study can be rationalized in a system-by-system manner. In the Nb–Ni–O system the two phases Nb_4Ni_2O and Nb_6Ni_6O occur. This occurrence was not observed in the Zr–Ni–O system. The phase diagrams of the binary intermetallic Zr–Ni and Nb–Ni systems are very different. In the Nb–Ni binary system there are only two compounds, $NbNi_3$ and Nb_7Ni_6, which compete with formation of the ternary oxide. In neither case is the Nb:Ni ratio 1:1 or 2:1. The binary intermetallics in the Zr–Ni system, especially ZrNi, compete more favorably with the formation of the ternary oxide. One can consider the role of oxygen in stabilizing the Ti_2Ni-type structure in the Zr_4Ni_2O phase. The oxygen is also necessary in the formation of the Hf_4Ni_2O phase [7], but is not necessary for Ti_2Ni. A principal difference between titanium on the one hand, and zirconium and hafnium on the other, is the orbital expansion of the d orbitals for zirconium and hafnium and the corresponding increase in metal–metal bond strength. Compare, for example, the heats of

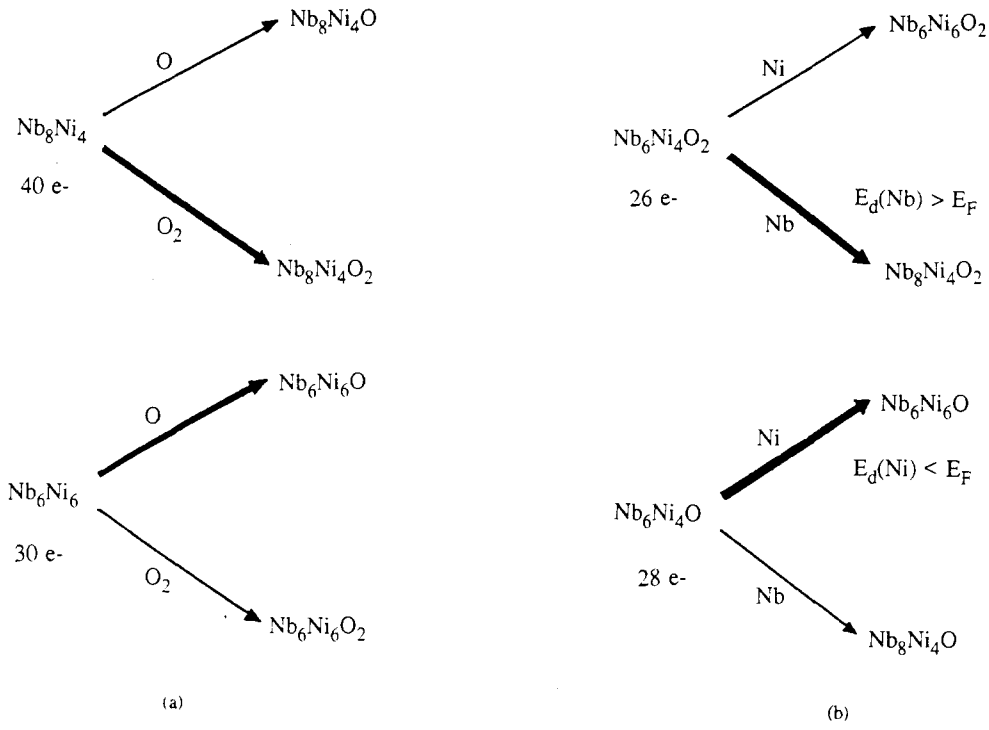

Fig. 4. (a) Addition of oxygen to hypothetical metal framework follows path shown by bold arrows. (b) Addition of capping metal atoms to core compounds follows path shown by bold arrows.

formation of the gaseous atoms at 0 K, which may be regarded as a measure of the cohesive energy of the metals. For Ti, $\Delta H_f^\circ(0\ \mathrm{K}) = 111.65$ kcal mol^{-1}, and the values for Zr and Hf are 145.19 kcal mol^{-1} and 147.92 kcal mol^{-1} respectively [36]. The phases in the Zr–Ni system are different from those in the Ti–Ni system because the bonding energies of zirconium and titanium differ. Specifically Zr_2Ni and Ti_2Ni crystallize with different structures. When oxygen is added to Zr_2Ni, zirconium–oxygen bonds form at the expense of the zirconium–metal bonds. This decrease in metal–metal bonding makes Zr–Ni more like the Ti–Ni system, and the filled-Ti_2Ni phase in the Zr–Ni–O system is stabilized with respect to the binary phases.

The oxygen occupancy in the Nb_4Ni_2O phase has not been determined experimentally, but is based on the assumption that the oxygen occupancy in this phase is the same as for $Nb_6Ni_4Ta_2O_2$. The two phases Nb_6Ni_6O and Nb_4Ni_2O have different Nb:Ni ratios and different oxygen contents. The band calculations on Nb_6Ni_6O suggest the ordering of the oxygen may not be as important as the total amount of oxygen present. Figure 4(a) outlines the possibility of adding different amounts of oxygen to metal frameworks with different Nb:Ni ratios. With reference to the DOS curve in Fig. 3, the electrons in the sharp Ni d peak are strongly localized. The electrons occupying the Zr d, s and p bands, and Ni s and p bands, are more delocalized. The core metal framework with the greater number of delocalized electrons in the conduction band will favor adding more oxygen, which acts as an electron sink, nominally forming O^{2-}. Nb_8Ni_4 contains 40 delocalized electrons per formula unit, and Nb_6Ni_6 has 30 electrons. Thus Nb_8Ni_4 will add more oxygen atoms per formula unit than Nb_6Ni_6 to form $Nb_8Ni_4O_2$ and Nb_6Ni_6O respectively.

The same conclusion is reached if the oxygen ordering is assumed to determine the metal ratios, rather than the metal ratios determining the oxygen ordering as described above. In this case, the two core compounds with different oxygen contents, Nb_6Ni_4O and $Nb_6Ni_4O_2$, can add either niobium or nickel to the 16d site (Fig. 4(b)). Nb_6Ni_4O has 28 delocalized electrons in its conduction band, and $Nb_6Ni_4O_2$ has 26. Since Nb_6Ni_4O is more electron rich it will more readily add nickel, for which atomic orbitals lie lower in energy than the Fermi level and will act as electron acceptors, than gain electrons by adding niobium to form Nb_6Ni_6O. $Nb_6Ni_4O_2$, with fewer delocalized electrons, will favor the addition of niobium, for which the orbitals lie above the Fermi energy and will act as electron donors to form $Nb_8Ni_4O_2$, or Nb_4Ni_2O. While this explanation is internally consistent in that the same conclusion is reached whether the oxygen content is considered to determine the metal occupancy, or the metal ratios determine the oxygen content, it does not explain the formation of phases such as Mo_6Co_6C and $Mo_6Co_6C_2$ where both possible orderings of interstitials are observed for a single metal ratio [6].

The formation of only $Nb_6Ni_4Ta_2O_2$, and no other tantalum-containing compounds, can be explained on the basis of work on mixed niobium–tantalum sulfides performed previously in this laboratory [16, 17]. In these sulfides, the formation of certain phases depends on the relative strengths of metal–sulfur bonds and metal–metal bonds. The same interplay between metal–oxygen and metal–metal bonds exists in these oxide phases. Generally speaking, Ta–O bonds are stronger than Nb–O bonds, by electronegativity arguments. Also, Ta–M bonding among transition metals is generally stronger than Nb–M bonds in a given structure, because of greater d orbital extension and overlap of 5d transition metals. In the Ti_2Ni-type structure one must consider the balance between the M–O and the M–M bonding. In Nb_4Ni_2O the oxygen is surrounded by niobium in the 48f site, forming Nb_6O octahedra. The other niobium atom has only other metal atoms as neighbors; it is icosahedrally coordinated to six nickel and six niobium atoms. When tantalum replaces niobium in the 16d site, oxygen still is coordinated to only niobium, but now the presence of tantalum increases the metal–metal interactions in the structure. If, however, tantalum were to replace the other niobium atoms, the stronger Ta–O bonds would come at the expense of the Ta–M bond strength, shifting the balance of metal–oxygen *vs.* metal–metal bond strength, and the phase is unstable with respect to formation of the binary phases.

6. Conclusions

Structural determination of these new phases by single-crystal X-ray diffraction techniques gives evidence for three different orderings of the interstitial oxygen. Zr_4Ni_2O and $Nb_6Ni_4Ta_2O_2$ contain oxygen in the 16c site. Nb_6Ni_6O contains oxygen in the 8a site. The oxygen in $Zr_6Ni_4Ti_2O_{0.6}$ partially occupies both the 8a and the 16c sites. The octahedral site around oxygen is expanded, and this is noted in a shift of the positional parameter of the Zr or Nb atom on the 48f site. This correlation is very useful, as powder X-ray diffraction is better able to determine metal atom positions than to distinguish between possible interstitial site occupancies. The metal atoms in the quaternary compounds selectively occupy unique sites.

Acknowledgments

Magnetic measurements were done by Dr. J. Ostenson. EDS work was performed by Dr. W. Strazsheim. The Ames Laboratory is operated for the US Department of Energy by Iowa State University under Contract W-7405-Eng-82. This research was supported by the Office of the Basic Energy Sciences, Materials Sciences Division, DOE, and, partially, by the Donors of the Petroleum Research Fund administered by the American Chemical Society.

Supplementary material available

Anisotropic displacement parameters (1 page) and a listing of structure factor data (4 pages) are available from the authors.

References

1 A. Westgren and G. Phragmén, *Trans. Am. Soc. Steel Treat., 13* (1928) 539.
2 M.V. Nevitt, in J.H. Westbrook (ed.), *Intermetallic Compounds,* Wiley, New York, 1967.
3 P. Villars and L.D. Calvert (eds.), *Pearson's Handbook of Crystallographic Data for Intermetallic Phases,* American Society for Metals, Materials Park, OH, 2nd edn., 1991.
4 K. Kuo, *Acta Metall., 1* (1953) 301.
5 W. Jeitschko, H. Holleck, H. Nowotny and F. Benesovsky, *Monatsh. Chem., 95* (1964) 1004.
6 J.M. Newsam, A.J. Jacobson, L.E. McCandlish and R.S. Polizzotti, *J. Solid State Chem.,, 75* (1988) 296.
7 M. Kotyk and H.H. Stadelmaier, *Metall. Trans., 1* (1970) 889.
8 H. Holleck and F. Thümmler, *Montash. Chem., 98* (1967) 133.
9 D.S. Bem, C.P. Gibson and H.-C. zur Loye, *Chem. Mater., 5* (1993) 397.
10 M.V. Nevitt, J.W. Downey and R.A. Morris, *Trans. Metall. Soc. AIME, 218* (1960) 1019.
11 N. Karlsson, *Nature (London), 168* (1951) 558.
12 S.R. Leonard, B.S. Snyder, L. Brewer and A.M. Stacy, *J. Solid State Chem., 92* (1991) 39.
13 F. Bonhomme, P. Selvam, M. Yoshida, K. Yvon and P. Fischer, *J. Alloys Comp., 178* (1992) 167.
14 B. Rupp and P. Fischer, *J. Less-Common Met., 144* (1988) 275.
15 M.H. Mueller and H.W. Knott, *Trans. Metall. Soc. AIME, 227* (1963) 674.
16 X. Yao, G. Marking and H.F. Franzen, *Ber. Bunsenges Phys. Chem., 96* (1992) 1552.
17 X. Yao, G.M. Miller and H.F. Franzen, *J. Alloys Comp., 183* (1992) 7.
18 L. Bsenko, *J. Less-Common Met., 63* (1979) 171.
19 G.M. Sheldrick, in G.M. Sheldrick, C. Krüger and R. Goddard (eds.), *Crystallographic Computing 3,* Oxford Unviersity Press, London, 1985, pp. 175–189.
20 TEXSAN: *Single Crystal Structure Analysis Software,* Version 5.0, Molecular Structure Corporation, The Woodlands, TX, 1989.
21 R. Mackay and H.F. Franzen, *J. Alloys Comp., 186* (1992) L7.
22 R. Mackay and H.F. Franzen, *Z. Anorg. Allg. Chem., 616* (1992) 154.
23 R. Mackay and H.F. Franzen, *Chem. Mater., 5* (1993) 857.
24 M.V. Nevitt and J.W. Downey, *Trans. Metall. Soc. AIME, 221* (1961) 1014.

25 B.G. Hyde and S. Andersson, *Inorganic Crystal Structures*, Wiley, New York, 1989.
26 W.C. Hamilton, *Acta Crystallogr., 18* (1965) 502.
27 H.H. Stadelmaier and M.-L. Fiedler, *Z. Metallkd., 66* (1975) 224.
28 H. Basch and H.B. Gray, *Theor. Chim. Acta, 4* (1966) 367.
29 J.W. Richardson, W.D. Nieuwport, R.R. Powell and W.F. Edgell, *J. Chem. Phys., 36* (1962) 1057.
30 V.I. Baranovskii and A.B. Nikoskii, *Teor. Eksp. Khim., 3* (1967) 527.
31 F. Herman and S. Sillman, *Atomic Structure Calculations*, Prentice-Hall, Englewood Cliffs, NJ, 1963.
32 R. Hoffmann, *J. Chem. Phys., 39* (1963) 1397.
33 A. Simon, H.-J. Mattausch, G.J. Miller, W. Bauhofer and R.K. Kremer, *Handbook on the Physics and Chemistry of Rare Earths*, Vol. 15, Elsevier, Amsterdam, 1991, Chap. 100.
34 P. Rogl and H. Nowotny, *Monatsh. Chem., 108* (1976) 1167.
35 H.G. von Schnering and R. Nesper, *Angew. Chem. (Int. Edn. Engl.), 27* (1987) 1059.
36 R.C. Weast (ed.), *CRC Handbook of Chemistry and Physics*, CRC Press, Boca Raton, FL, 65th edn., 1984, p. D-50.